Electronic Supplementary Material – Hydrogeology Journal

Integrated hydrogeological modelling of hard-rock semi-arid terrain: supporting sustainable agricultural groundwater use in Hout catchment, Limpopo Province, South Africa

Girma Y. Ebrahim[1, *], Karen G. Villholth[1], Maurice Boulos[1, 2]

[1] International Water Management Institute, 141 Creswell Road Weavind Park, Silverton, Pretoria, South Africa,

[2]Swiss Federal Institute of Technology Zurich, Switzerland

[*]Corresponding author email: g.ebrahim@cgiar.org

Contents

S1. Soil type and texture classes 2
S2. Crop consumptive use 3
S3. Weathering depth 4
S4. Initial conditions 5
S5. Rainfall distribution in the catchment area 8
S6. Crop-related data 9
S7. Irrigated area 11
S8. River - aquifer interactions 14
S9. Precipitation-Runoff Modelling System 17
S10. Sensitivity analysis 21
S11. MODFLOW-OWHM model calibration and validation 22
S12. Evapotranspiration from groundwater 24

S1. Soil type and texture classes

Soil type for the Hout catchment was determined from the Soil Atlas of Africa (Fig. S1). The percentage area covered by each soil type and descriptions are presented in Table S1. The main soil type in the area is Luvisols, which accounts for 56.5% of the catchment area. The Cambisols represent soils along the drainage networks. Soil texture classes and spatial distribution were determined using the global soil dataset (SoilGrids, 1 km, http://www.soilgrids.org/index.html). The main soil texture class in the Hout catchment is sandy soil.

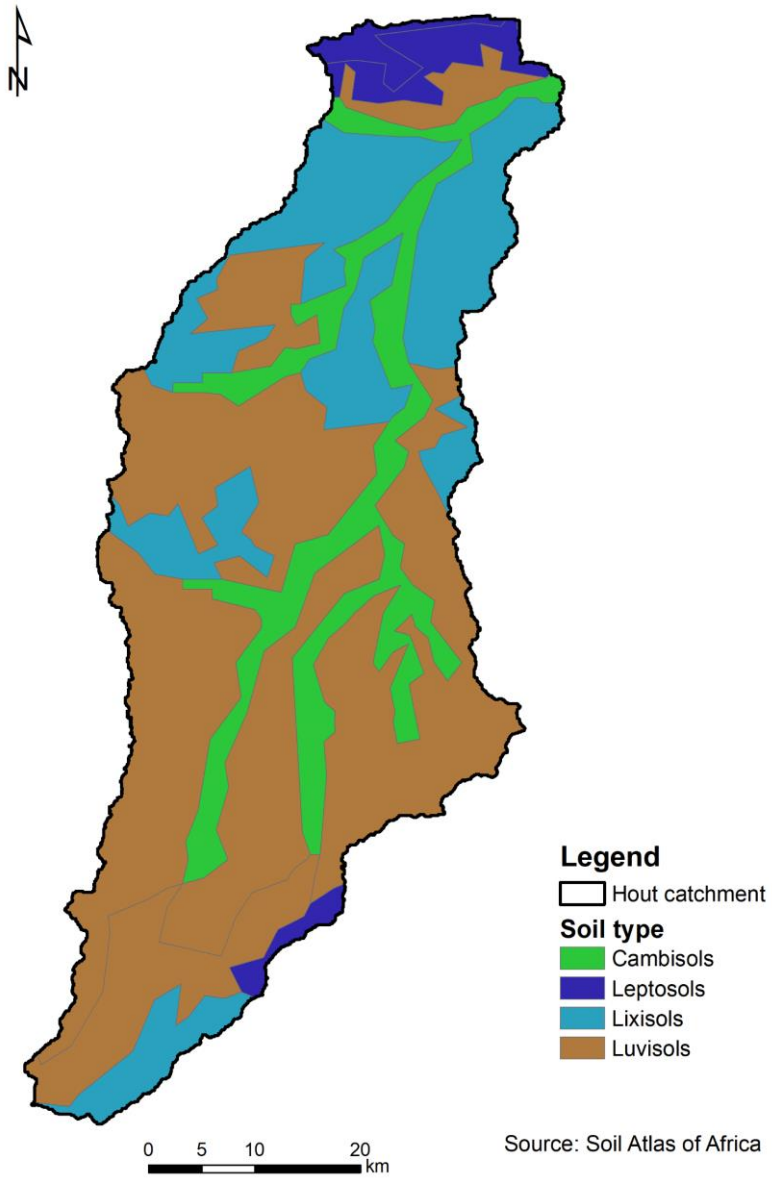

Fig. S1. Soil type of the Hout catchment (Source: Soil Atlas of Africa (Jones et al., 2013)).

Table S1. Percentage of area covered by different soil types and descripitons from Soil Atlas of Africa (Jones et al., 2013).

Soil reference group name	Description	Area (km^2)	% area covered by each soil type
Cambisols	Soil that is only moderately developed on account of limited age (from Latin *cambiare*, to change)	376.84	15.21
Leptosols	Shallow soil over hard rock or gravelly material (from Greek leptos, thin).	121.66	4.91
Lixisols	Slightly acid soils with a clay-enriched subsoil and high nutrient-holding capacity (from Latin luere, to wash).	579.59	23.39
Luvisols	Slightly acid soils with a clay-enriched subsoil and low nutrient-holding capacity (from Latin lixivia, washed-out substances)	1400.28	56.50

S2. Crop consumptive use

MODFLOW-OWHM has two options for calculating crop consumptive use. Consumptive use concept 1 represents a step-wise linear approximation for transpiration for groundwater levels between the bottom of the root zone and ground surface. When the groundwater level is at the root zone, maximum transpiration occurs, and when the groundwater level rises above the root zone, transpiration is restricted by anoxia condition. The depths within the root zone that correspond to user-specified crop-specific anoxia or wilting-related pressure heads are calculated using analytical solutions for a vertical steady state pressure-head distribution over the depth of the root zone.

Consumptive use concept 2, which is used in this study, is a relatively simple conceptual model (Fig. S2). For a groundwater level equal to the bottom of the root zone, the maximum actual crop transpiration and the maximum actual transpiration from groundwater are equal to the potential crop transpiration. As the groundwater level rises above the bottom of the root zone, a linear decrease in transpiration is assumed. As the groundwater level drops below the bottom of the root zone, the actual transpiration from groundwater is assumed to decrease linearly from the respective maximum actual transpiration from groundwater (at the bottom of the root zone) to a transpiration extinction depth (thickness of capillary fringe below the root zone). The evaporation from groundwater over exposed non-cropped areas is assumed to decrease linearly with the groundwater level, from the maximum actual

evaporation from groundwater, when the highest point of the capillary fringe is at the ground surface, to an evaporation from groundwater extinction depth (thickness of the capillary fringe below the ground surface).

The extinction level for groundwater transpiration is calculated as ground-surface elevation minus (root zone depth + capillary fringe). If the water table is below the root length and capillary fringe, it is assumed that there is no transpiration or uptake from groundwater. Extinction level for groundwater evaporation is the ground surface minus the capillary fringe.

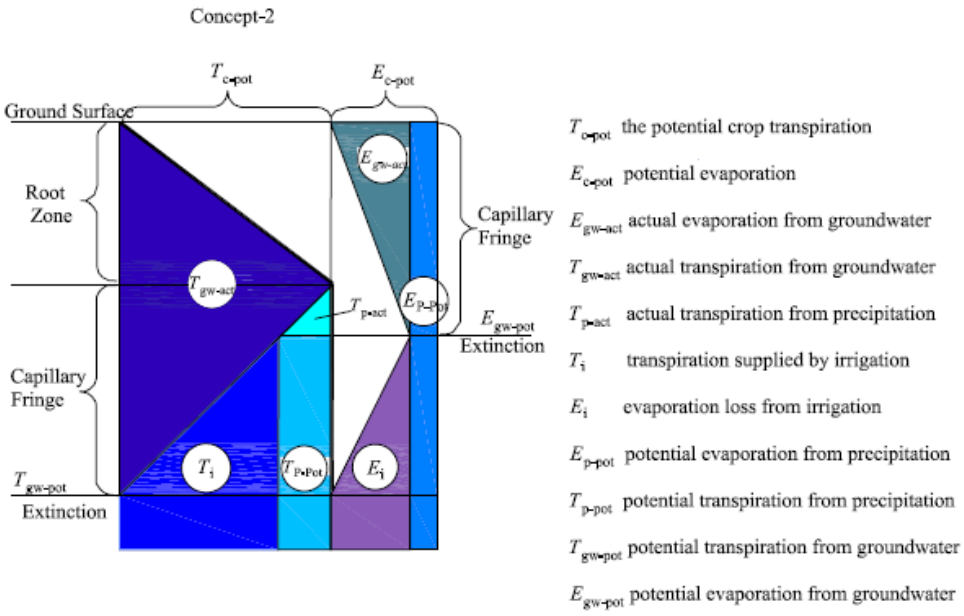

Fig. S2 Conceptual approximations to change of crop consumptive use components with varying head (concept 2). Reproduced from the User guide for the farm process (FMP1) package (Schmid et al., 2006)

S3. Weathering depth

The kriging method was used to interpolate depth of weathering (Fig. S3). In total 38 well logs from the National Groundwater Archive (NGA) were used for interpolation. Weathering depth in the 38 well-log data ranges from 30 to 90 m with mean of 46.7 m.

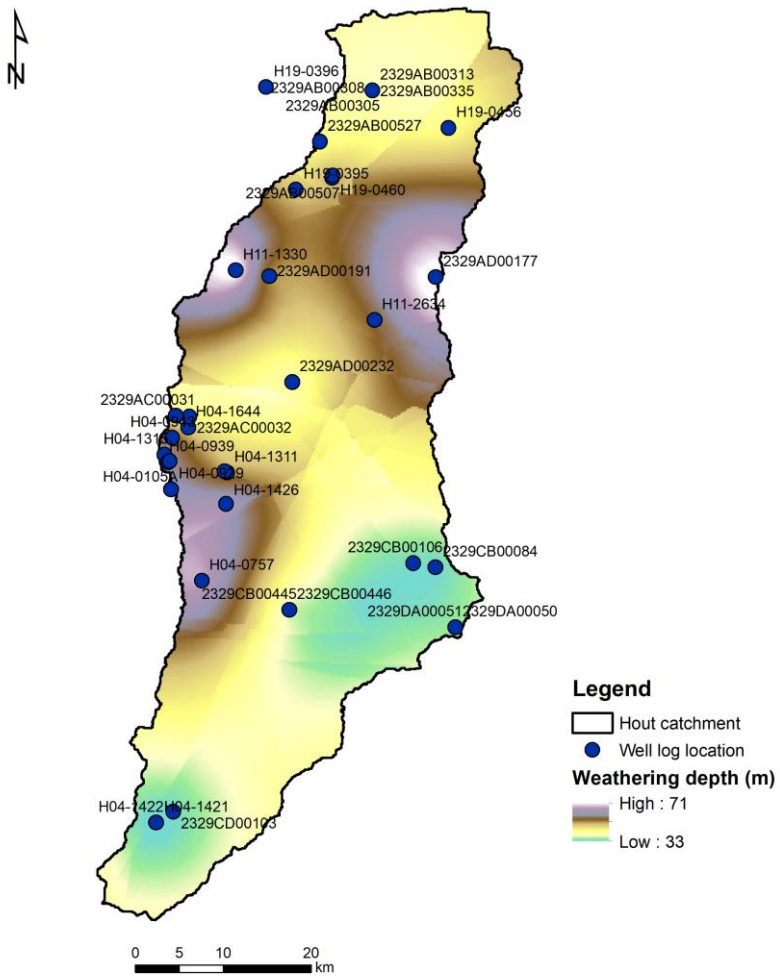

Fig. S3. Weathering depth interpolated using kriging based on 38 well log data

S4. Initial conditions

The groundwater flow component of the MODFLOW-OWHM model is represented using the transient 3-D groundwater flow equation (Harbaugh, 2005) (Eqn. (S1)),

$$\frac{\partial}{\partial x}\left(K_x \frac{\partial h}{\partial x}\right) + \frac{\partial}{\partial y}\left(K_y \frac{\partial h}{\partial y}\right) + \frac{\partial}{\partial z}\left(K_z \frac{\partial h}{\partial z}\right) - W = \mathrm{Ss}\frac{\partial h}{\partial t} \qquad \text{(S1)}$$

Where K_x, K_y, and K_z are hydraulic conductivities in x, y, and z directions (L/T), h is hydraulic head (L), t is time (T), W is a source-sink term (1/T) representing recharge, pumping, evaporation, etc., and Ss is specific storage (1/L), which when multiplied by the saturated thickness gives the confined aquifer storage coefficient, S (-), or the unconfined aquifer specific yield Sy (-).

Equation (S1) is solved in MODFLOW-OWHM using back-ward finite difference. Hence, it requires head distribution (water level) at the beginning of the time steps to calculate the head distribution at the end of the time steps. For each time step, the head distribution at the start of one time step is set equal to the head distribution at the end of the previous time step. This chain of water level calculations is started from user-specified initial head values, which is commonly known as initial conditions. Initial conditions are not used after the first time step to calculate water level and do not have influence on steady state simulation, however, this affects transient model simulation with a fading effect as time progresses. Incorrect initial head may results in an extreme (large or small) volume of water being stored in the aquifer, and when simulations are performed with this initial head, the flow condition will be dominated by the wrong positioned water and mask the influences of recharge and abstractions (Lloyd, 1981). Initial head and storage coefficients have been shown to be negatively correlated (Liu et al., 2009). According to Anderson and Woessner (2002), model-generated initial conditions provide better consistency between the initial head data and the model hydrologic inputs and parameters than field-interpolated head values.

The classical approach for defining initial head for transient model simulations follows a two-step procedure, whereby firstly a steady state model is calibrated for a pre-development time period, and secondly using the output of the steady state model as initial head for transient simulation. However, if the aquifer has long been under transient conditions, or the data for specifying the initial head are limited, true steady state may not be achieved in the first step. In this case, an alternative approach has to be followed, in which the transient model is run for a sufficiently long time so that the influence of the initial conditions is minimized (Lemieux et al., 2008) prior to the actual simulation. This initial phase is known as the spin-up period, in which the simulated hydrology is brought to dynamic equilibrium with a metrological forcing through iterative simulations (Ajami et al., 2015). The rationale behind this selection of initial conditions is that the influence of the initial conditions diminishes as the simulation progresses, so errors associated with selecting possibly erroneous initial conditions will be small provided sufficient simulated time has elapsed.

For the present study, initial conditions were defined using the second method described above. Interpolated observed water level data measured for the year 2005-2007 in 69 wells were interpolated using kriging (Fig. S4). It is important to note that 46 out of the 69 water level data were obtained from GRIP Limpopo database pumping well data (http://griplimpopo.co.za/). Most of the water level data were taken from hand pump wells, hence the effect of pumping on the groundwater level data is minimal. Since, not all wells have water level data for the year 2007, water level data monitored during 2005 and 2006 were used in the interpolation assuming that the annual

variability in water level is small. In observation wells for which monitoring started after 2007, correlation with the nearest observation borehole using recent data was used to obtain water level for year 2007. To remove errors introduced during interpolation and inconsistency between initial condition and model parameters, the transient model for year 2007 was run repeatedly six times using a one-year annual cycle to iteratively establish dynamic equilibrium as demonstrated by Barlow and Dickerman (2001).

A General Head Boundary (GHB) was specified at the catchment outlet based on observed water level data at monitoring well A7N0019. The depth to groundwater in A7N0019 ranges from 4.7 to 14.9 m below the ground surface. Elevation difference between A7N0019 (elevation =855 mamsl) and the lowest point of the GHB (where the river crosses the GHB, elevation 831.15 mamsl) is 23.5 m. To account for elevation difference and water level gradient, the water level at A7N0019 was lowered by 37.7 m and used to define water level at GHB cells. This results in a positive outflow though the GHB. If the water level at A7N0019 was used directly to define GHB, the water level downstream of the catchment outlet is higher than simulated level in the cells upstream of the GHB. This results in flow into the catchment, as opposed to leaving through the GHB, which is not realistic.

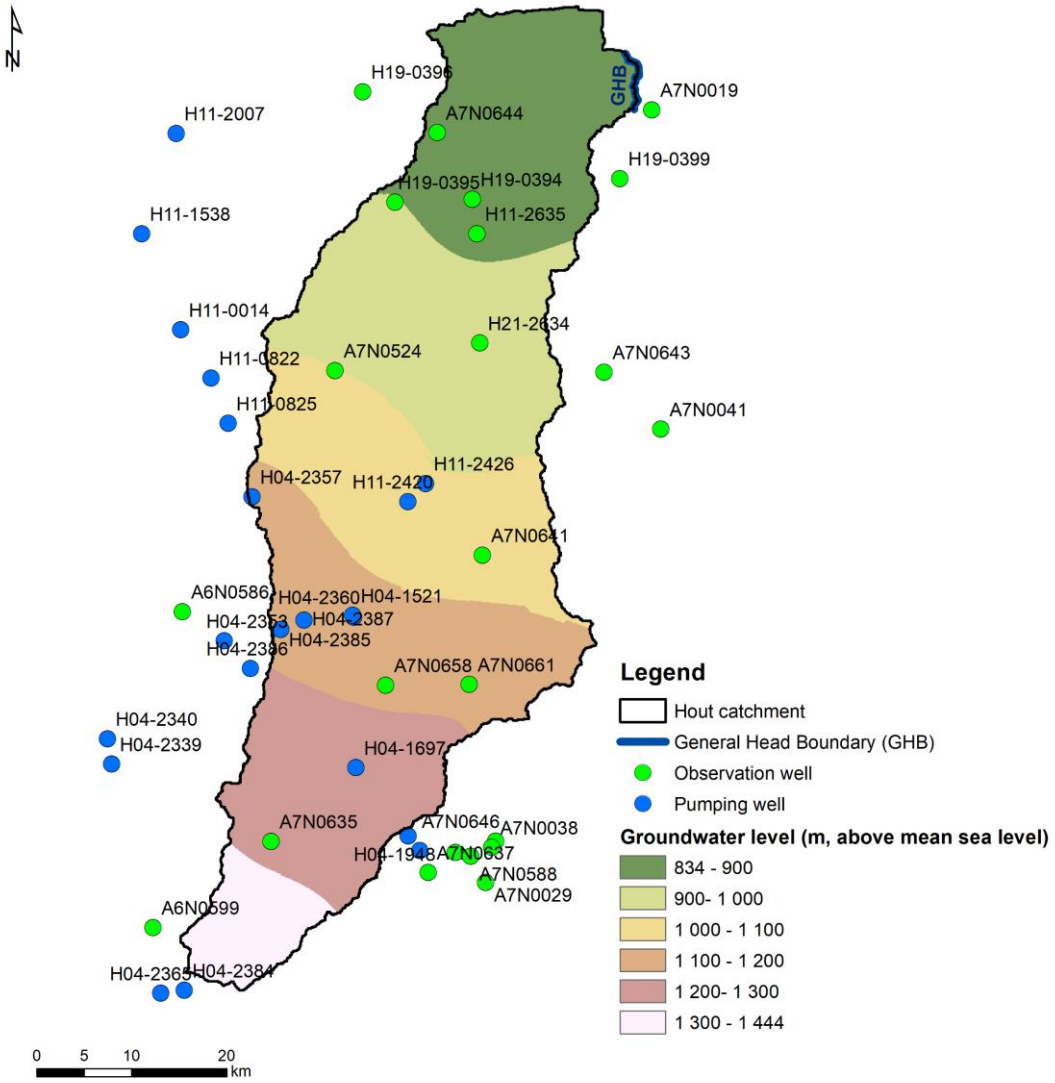

Fig. S4. Location of 69 wells (23 observation wells and 46 pumping wells), interpolated water level used as initial condition, observation well (A7N0019) used to define the general head boundary, and location of the general head boundary.

S5. Rainfall distribution in the catchment area

The Thiessen polygon method is probably the most common method used in hydrology for determining areal precipitation distribution. In the present study, six rainfall stations (Fig. S5) were used to obtain spatially distributed monthly rainfall values used in the model. The Thiessen polygon networks were imported as a shape file and for each polygon, monthly rainfall time series data are assigned from the closest rainfall station. As shown, the Dendron rainfall station covers the largest part of the catchment area (about 47%).

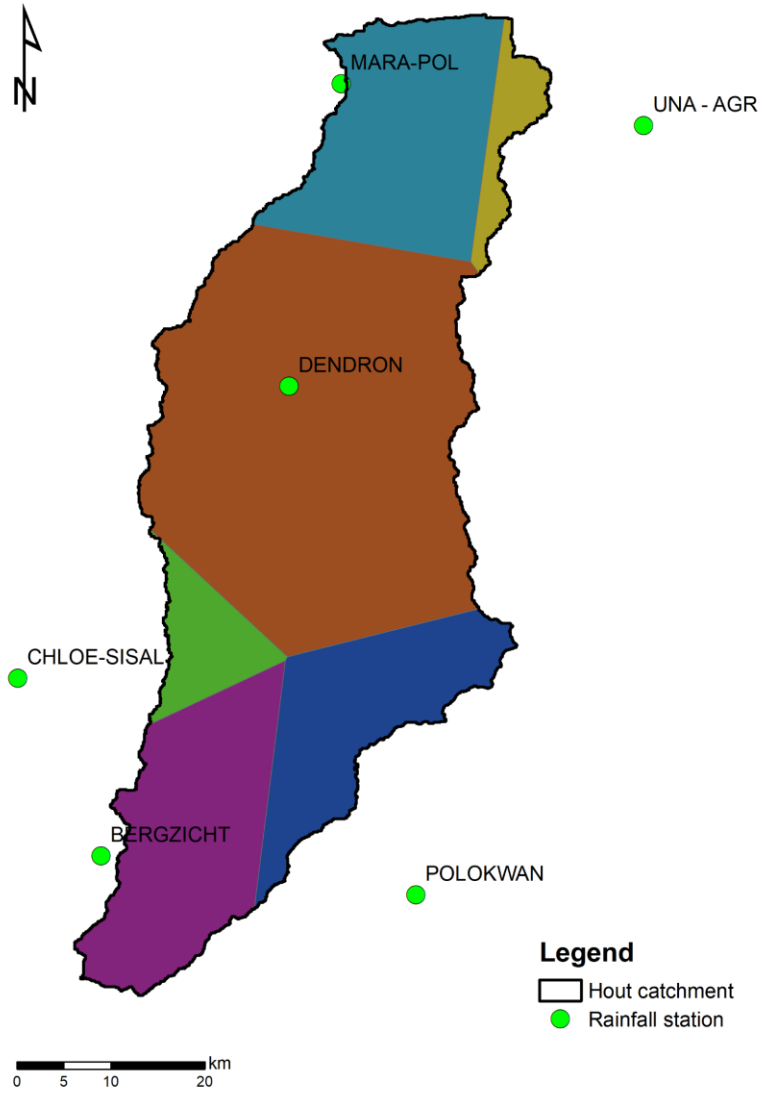

Fig. S5. Rainfall stations and Thiessen polygon coverages

S6. Crop-related data

For all land uses, the model needs the following input parameters: (i) Crop coefficient (kc); (ii) Transpiration fraction of consumptive use (k_T), evaporation fraction of consumptive use (k_E). Evaporation fraction from precipitation (k_E^P) is equal to 1-k_T, while evaporation fraction from irrigation (k_E^i) is less than 1-k_T; (iii) maximum root depth (RTD); and (iv) fractions of excess precipitation and irrigation that become surface runoff (IE_{SWP} and IE_{SWI}, respectively). The temporally varying crop coefficient and transpiration fraction of

consumptive use values for potato are presented in Fig. S6. Also, the composite kc for staggered planting of potato over the period Feb – July is shown. Standard constant values were applied for other land uses (Table S2). Maximum rooting depth, fractions of excess precipitation and irrigation that turn to surface runoff are also presented in Table S2. Maximum rooting depth and kc values for the urban areas are specified to represent small green spaces mainly covered by grass. For the waterbodies, these values are specified as placeholder zero values. IE_{SWP} is determined through manual model calibration (see Section 'MODFLOW-OWHM calibration and validation' in the main article), while all the other crop-specific parameters were derived from the literature.

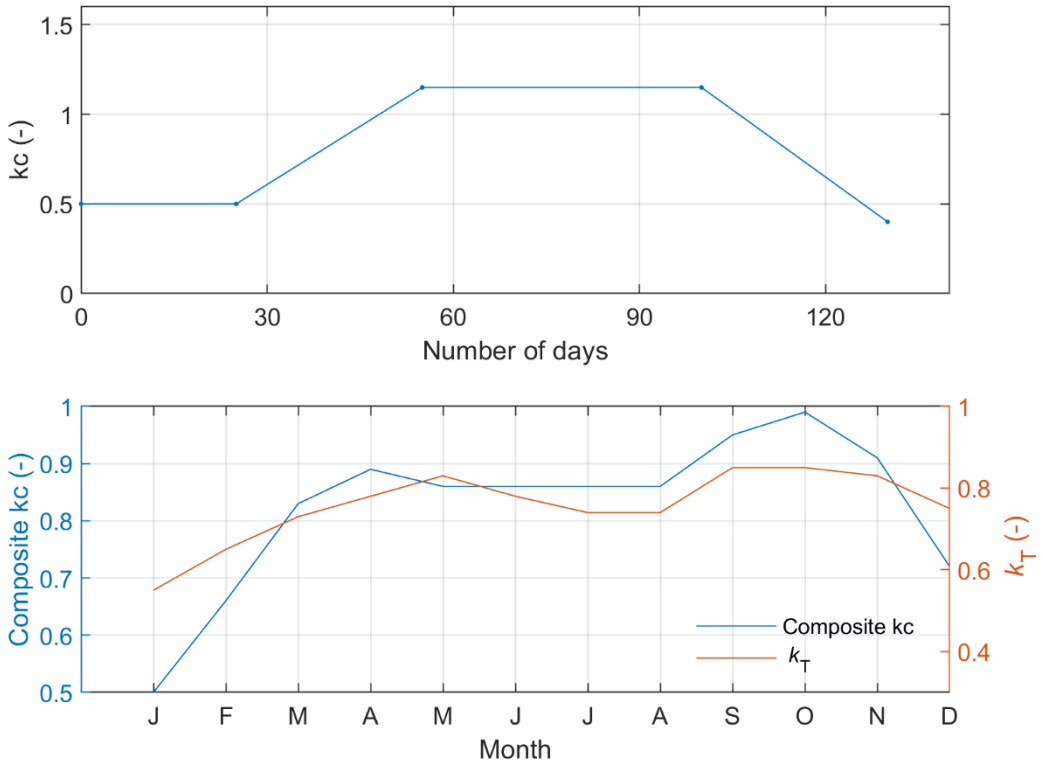

Fig. S6. Crop coefficient (kc) for the 4.5-month growing period of potato (top), and monthly composite kc and transpiration fraction of consumptive use (k_T) (bottom) (assuming that the planting season of potatoes is spread evenly over the period Feb-July).

Table S2. Maximum rooting depth (RTD), fraction of excess precipitation that turns into surface runoff (IE_{SWP}) and fraction of excess irrigation that becomes surface runoff (IE_{SWI}), crop coefficient (kc), transpiration fraction of consumptive use (k_T), fraction of evaporation from precipitation (k_E^P) and fraction of evaporation from irrigation (k_E^i).

Land use/land cover type	RTD (m)	IE_{SWP} (-)	IE_{SWI} (-)	kc (-)	k_T (-)	k_E^P (-)	k_E^i (-)
Potato [a]	0.60	0.165	0.004	0.78	0.72	0.28	0.15
Cultivated land (not potato)	0.60	0.5	0.00	0.9	0.55	0.45	0.00
Degraded land	1.50	0.5	0.00	1.2	0.65	0.35	0.00
Natural vegetation	2.00	0.5	0.00	1.2	0.85	0.15	0.00
Urban areas	0.10	0.2	0.00	0.1	0.25	0.75	0.00
Water bodies	0.00	0.00	0.00	0.0	0.0	1.00	0.00

[a] For pototo monthly mean kc, k_T and k_E^P values are presented. See also Fig. S6 for temporal variation of potato parameters.

S7. Irrigated area

Multi-temporal land use maps are not available for the Hout catchment. Hence, irrigated areas were delineated seasonally using multi-temporal Landsat images for the simulation period. Irrigated areas defined this way were assumed to be cropped with potatoes and overruled areas otherwise defined by the land use/land cover map. Irrigated areas were delineated using the Normalized Difference Vegetation Index (NDVI). Two Landsat images for every year were used to represent the two main cropping seasons (Table S3). The key issue of any NDVI-based methodology is the selection of an NDVI threshold, above which a particular pixel in the NDVI image is assumed to be irrigated. By trial-and-error, using a Landsat image dated 31-08-1986 and NDVI threshold of 0.13, an irrigated area of 1356 ha was calculated, which is very close to the irrigated area that was found by a survey conducted during the period of 28 July – 7 October 1986 (1370 ha) for Doringlaagte drainage basin, the most highly developed sub-basin of the Hout catchment (Jolly, 1986). However, the NDVI threshold during the simulation period was not constant and ranged from 0.13 to 0.4. This is because irrigated areas can be identified easily with a lower NDVI threshold during the dry season, but during the wet season natural vegetation and non-irrigated areas, which remain fallow, may have NDVI very similar to irrigated areas. Hence, during the wet season,

higher NDVI thresholds were used to distinguish irrigated areas from non-irrigated. Furthermore, a map of areas equipped for irrigation (from National Department of Agriculture, Forestry and Fisheries of South Africa) were used as a mask to exclude non-irrigated areas with higher NDVI values. An NDVI threshold of 0.5 was used to delineate irrigated area in Northern Tunisia using a Landsat image (Kallel et al., 2017). An NDVI threshold of 0.30-0.45 was used to delineate irrigated area in Afghanistan using Landsat-derived NDVI (Pervez et al., 2014).

The seasonally irrigated area delineated during the simulation period is presented in Table S4. The monthly areal rainfall for the Hout catchment for the year 2007 calculated based on the Thiessen polygon method and mean monthly NDVI for areas equipped for irrigation for the same year are shown in Fig. S7. Lack of enough rainfall, particularly during May-August, clearly makes irrigation necessary to compensate for the large moisture deficit. During the period of October – December, irrigated crops show maximum greenness at the same time when maximum rainfall occurs. The greenness does not necessarily reflect irrigation. However, it is possible that the available rainfall may not be enough to meet the crop demands and thus supplemental irrigation is necessarily.

Table S3. Landsat images used for delinating irrigated area.

Simulation period	Simulation year	Time of image for dry period	Image source for dry period	Time of image for wet period	Image source for wet period
Calibration period	2007	21.05.07	Landsat 4-5	*23.09.06*	Landsat 4-5
	2008	21.04.08	Landsat 4-5	03.08.08	Landsat 7
	2009	26.05.09	Landsat 4-5	25.10.09	Landsat 7
	2010	*26.05.09*	Landsat 4-5	26.09.10	Landsat 7
	2011	24.05.11	Landsat 7	13.09.11	Landsat 7
	2012	26.05.12	Landsat 7	01.10.12	Landsat 7
Validation period	2013	21.05.13	Landsat 8	26.09.13	Landsat 8
	2014	08.05.14	Landsat 8	28.08.14	Landsat 8
	2015	11.05.15	Landsat 8	16.09.15	Landsat 8

The overpass frequency of the Landsat satellite is 16 days, but data availability is limited by cloud cover. Landsat data from 23.09.2006 are used to represent the situation in the latter half of 2007, as there were no data to capture the agricultural peak during that year. Image date in italic represent the image taken from the previous year for the same period as there was no image, or the image was affected by cloud cover in that particular year. The dry period represents the period February-August and the wet period represents September- December.

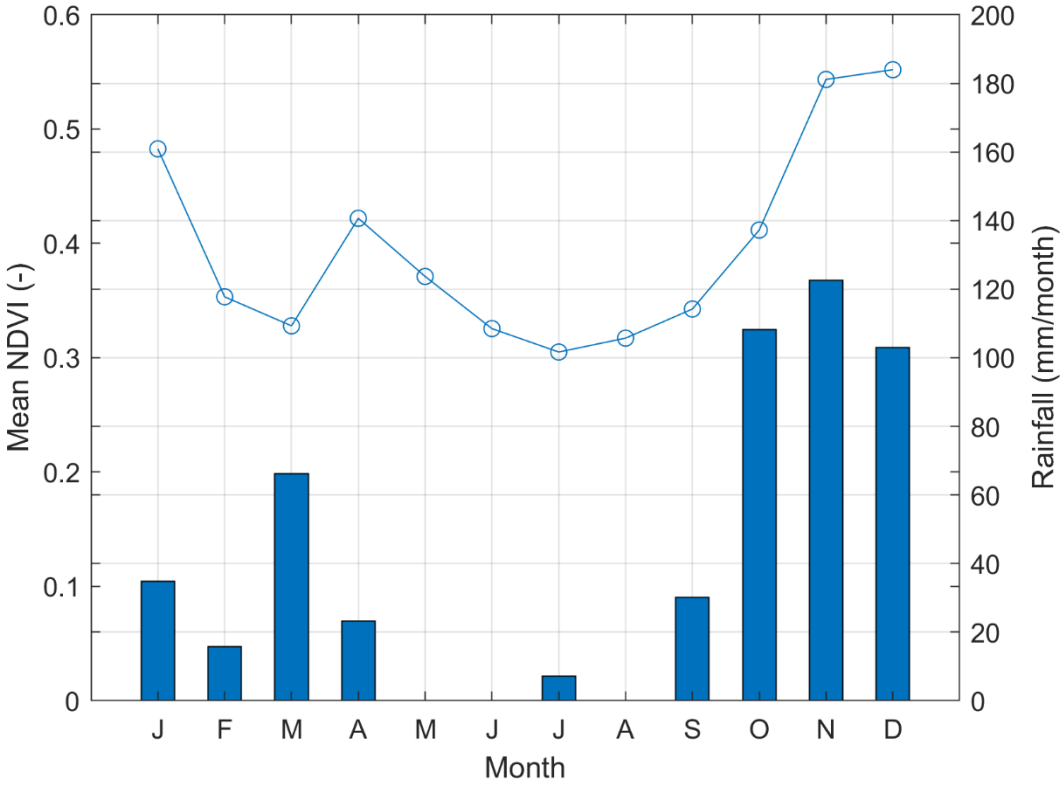

Fig. S7. Monthly areal rainfall of the Hout catchment for year 2007 calculated based on the Thiessen Polygon method and mean monthly NDVI for year 2007 for areas equipped for irrigation. Irrigation peak periods are during the relatively low rainfall periods that occur in April and September.

Table S4. Irrigated area during the simulation period.

Simulation period	Simulation year	Irrigated area, dry period (ha)	Irrigated area, wet period (ha)	Total irrigated area in a year (ha)
Calibration period	2007	2296	2537	4833
	2008	2337	2247	4584
	2009	2423	1788	4211
	2007	2296	2537	4833
	2011	2345	2424	4769
	2012	2363	2112	4475
Validation period	2013	2359	2269	4628
	2014	2306	2017	4323
	2015	2324	2368	4692
Mean irrigated area	-	2339	2225	4594
Standard deviation	-	40.4	249.0	220.8
Coefficient of variation in percent	-	1.7	11.2	4.8
Area actually irrigates as percentage of area equipped for irrigation		10.4	9.9	20.5
Area equipped for irrigation as percentage of total catchment area		9.0	9.0	9.0
Area actually irrigated as percentage of the total catchment area		0.9	0.9	1.9

Total catchment area is 2478 km^2 and area equipped for irrigation is about 224 km^2, which means about 9% of the catchment area is equipped for irrigation mainly by centre pivot irrigation system.

S8. River - aquifer interactions

River-aquifer flux exchange was simulated using the Streamflow Routing Package (SFR2) of MODFLOW (Niswonger and Prudic, 2005). SRF2 is the replacement of the Streamflow Routing (SFR1) Package developed for MODFLOW 2000 (Prudic et al., 2004). The main difference between the two packages is that SFR2 considers

the unsaturated zone between the streambed and aquifers. However, the present study did not simulate the unsaturated flow. SFR2 was selected because of package availability in the ModelMuse user graphic interface.

Flow between river and aquifer is modelled using the same approach as the standard River Package of MODFLOW. Flow is simulated using Darcy's Law using Eqn. (S2):

$$Q = \frac{K\,w\,l}{m}\,(h_s - h_a) \qquad \text{(S2)}$$

Where:

Q is a volumetric flow between given section of the stream and volume of the aquifer (L^3/T)

K is the hydraulic conductivity of the streambed sediments (L/T)

w is a representative width of the stream (L)

m is the thickness of the streambed deposit extending from the top to the bottom of the streambed (L)

l is the length of stream corresponding to a volume of aquifer length (L)

h_s is the head in the stream determined by adding stream water depth to the elevation of the streambed (L)

h_a is the head in the aquifer beneath the streambed (L)

The river channel network in SFR2 is divided into reaches and segments. A stream reach is a section of a stream that is associated with a particular finite difference cell. A stream segment is a group of stream reaches that have uniform properties such as 1) uniform rate of overland flow, precipitation and evapotranspiration, 2) uniform streambed thickness, hydraulic conductivity, stream cross-section and tributary inflow and outflows. Fig. S8 shows the five stream segments defined for the Hout catchment. Stream water depth is determined by application of Manning equation assuming a rectangular channel. Table S5 gives the model input data for the stream segments. Initial values of Manning roughness coefficients were determined from literature (Arcement and Schneider, 1989), and modified during model calibration. River cross-section, and upstream and downstream streambed elevations for each segment were determined from the 20 × 20 m Digital Elevation Model. Length of each segment was determined from the river channel shape file.

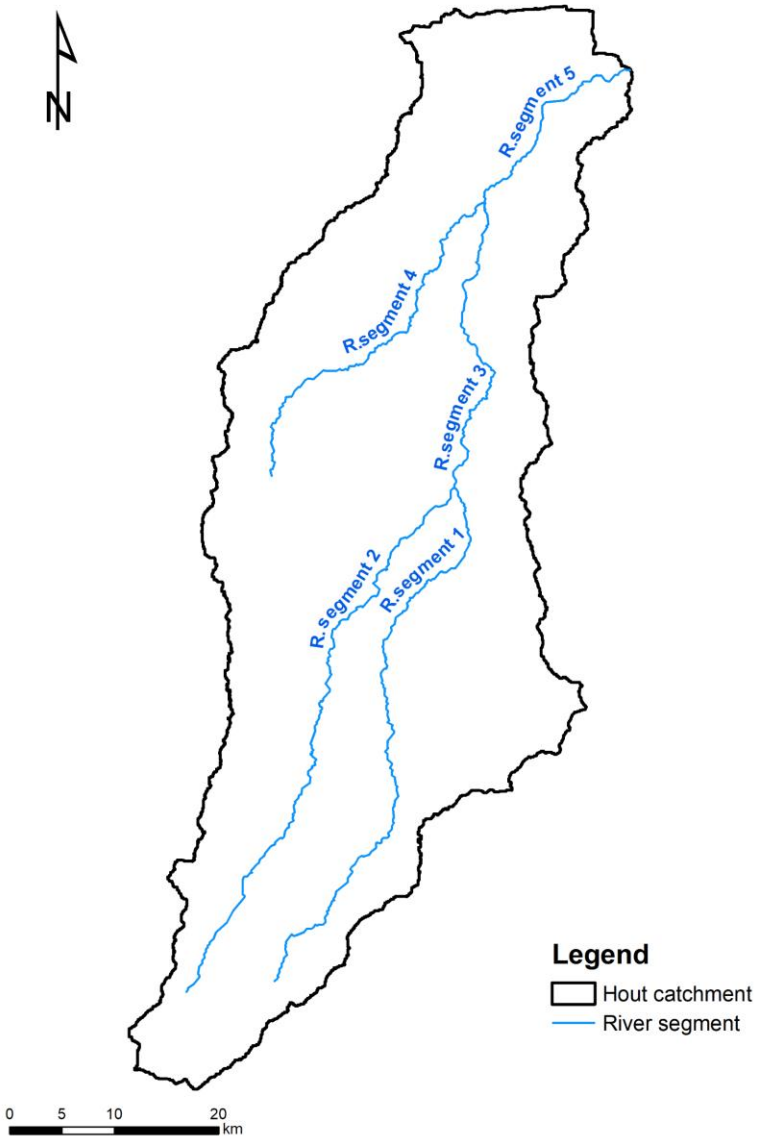

Fig. S8. Stream segments of the Hout River channels

Table S5. Stream segment input data

Stream segment ID	Stream bed elevation (upstream)	Stream bed elevation (downstream)	Stream length (km)/width (m)	River bed vertical hydraulic conductivity (m/d)	Manning roughness coefficient (-)
1	1324.6	1032.5	64.0/85	0.0145	0.1
2	1340.0	1032.5	65.8/41	0.0145	0.1
3	1025.1	904.7	35.2/129	0.0177	0.15
4	1068.2	904.7	42.8/21	0.0145	0.1
5	904.7	830.9	23.4/33	0.0177	0.15

S9. Precipitation-Runoff Modelling System

In the Precipitation-Runoff Modelling System (PRMS), the catchment is conceptualized by a number of hydrologically similar units, called hydrologic response units (HRUs). Each HRU is conceptualized as a parallel series of four reservoirs representing an impervious surface zone, the soil zone, the subsurface, and groundwater, whose outflows combine to produce surface runoff (Fig. 3 in the main article). The soil zone is divided into two layers. The upper layer is termed the recharge zone, and both evaporation and transpiration occur from this zone, while from the lower zone only transpiration takes place. The first attempt to satisfy potential evapotranspiration is made from the recharge zone. Subsurface discharge represents the relatively rapid discharge of water to streams and is conceptually similar to interflow. The groundwater system is conceptualized as a linear reservoir and is assumed the source of baseflow.

When soil zone storage reaches maximum water holding capacity, which is equal to the difference between field capacity and wilting point, additional infiltration is routed to the subsurface and groundwater reservoirs. Recharge to the groundwater reservoir is assumed to have a maximum daily limit. Water percolating from the soil zone first goes to the groundwater reservoir until the user-defined maximum recharge rate is exceeded. Recharge to the subsurface reservoir occurs when excess infiltration is exceeding the daily maximum recharge rate to groundwater. Recharge to the groundwater reservoir occurs from both the soil zone and subsurface reservoir. The maximum water holding capacity of the soil zone is one of the critical parameters, which determines the timing and volume of recharge to subsurface and groundwater reservoirs. This is because, for water to move from the soil zone to these zones, the soil moisture in the soil zone has to exceed the maximum water holding capacity.

The daily maximum recharge rate to the groundwater reservoir affects the distribution of subsurface and groundwater flow. Outflow from the groundwater reservoir that leaves the model domain is represented as a groundwater sink, which no longer contributes to streamflow.

Total daily precipitation depth received on an HRU is computed by multiplying the daily precipitation depth observed in the precipitation gauge associated with the HRU by a correction factor for the HRU. The correction factor is applied to account for the influence of elevation, spatial variation, topography, and gauge catch efficiency. Interception is computed as a function of the vegetation cover density and the leaf storage available for the predominant vegetation in an HRU. Net precipitation is computed by subtracting interception storage from total precipitation. Intercepted rain is assumed to evaporate at a free water-surface rate. Daily infiltration volumes are calculated as the difference between net precipitation and surface runoff. Surface runoff is computed using a contributing area concept. PRMS has the capability to compute daily potential evapotranspiration using seven different ways (Markstrom et al., 2015). Actual evapotranspiration is computed in the model using the assumption that the fraction of potential evapotranspiration that becomes actual evapotranspiration is a function of the ratio of available soil moisture to field capacity for three general soil types: sand, loam, and clay. For detailed explanations about the PRMS model, readers are referred to Leavesley et al. (1983) and Markstrom et al. (2015).

For this study, HRUs were delineated based on topography (Shuttle Radar Topography Mission (SRTM) 90 x 90 m Digital Elevation Model (DEM)) using a Geographic Information System (ArcGIS 10.4), and this resulted in 59 HRUs (Fig. S9). For each HRU, a water balance of unit flows and storages is computed each day and the sum of the water balances of all HRUs, weighted by HRU area, produces the daily watershed response. HRU characteristics, such as size, elevation, slope and aspect, were calculated from the DEM. Based on the dominant land cover, each HRU was assigned one of the four vegetation cover classes (bare soil, grasses, shrubs, and trees). Based on Hassan et al. (2014), vegetation cover densities for each HRU for the dry and wet season were calculated using NDVI maps representing the two seasons. The non-linear variable source area method was selected in the model for subsurface runoff simulation. Daily potential evapotranspiration is calculated as the product of daily pan evaporation data from Polokwane metrological station and user-defined monthly pan coefficients.

The model is calibrated using the Nash-Sutcliffe efficiency performance measure (Nash and Sutcliffe, 1970). Model parameters used during calibration, parameter ranges and calibrated values are presented in Table S6. epan_coef was varied monthly and the annual mean is presented in Table S6. The effects of four dams, shown in Fig. S9, were included in the model using the surface-depression process. Dams are not represented separately as

an HRU, rather they are used to define the fraction of HRU that can store water. The area of each dam was digitized from Google Earth images. The fraction of open surface depression storage area that can generate surface runoff as a function of storage volume within HRU (dprst_fact_open), and the fraction of open depression storage above which surface runoff occurs (op_flow_thres) were set to zero, and the fraction of pervious surface runoff that flows into depression storage (sro_to_dprst) was set to 0.8.

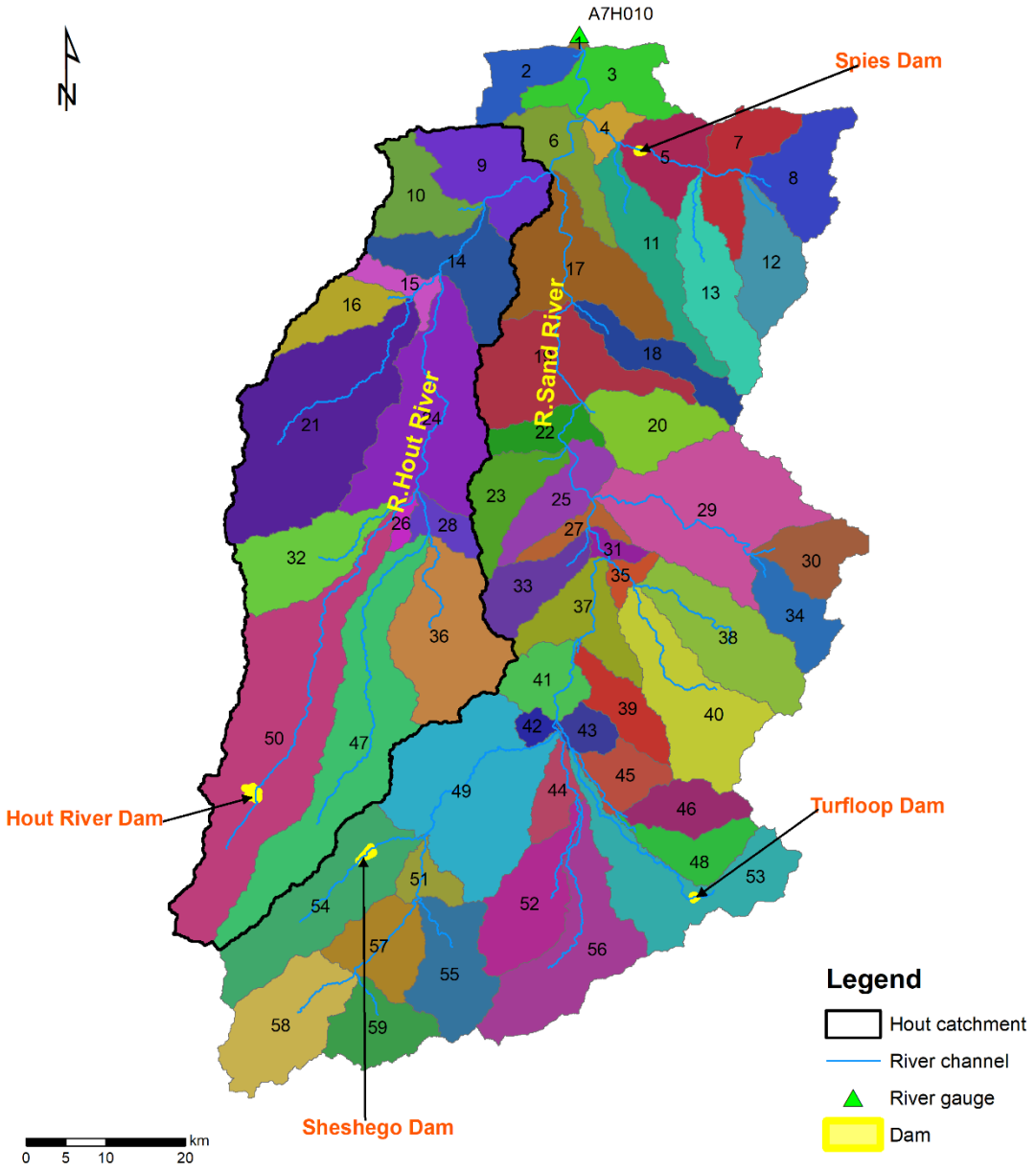

Fig. S9. Hydrological response units (HRUs) for Sand River catchment (59 HRUs delineated based on topography are shown as coloured polygons).

Table S6. PRMS model parameters and calibrated values

Parameter	Description	Units	Acceptable range	Calibrated value
carea_max	Maximum possible area contributing to surface runoff expressed as a portion of the HRU area	decimal fraction	0.8-1.0	0.82
epan_coef	Monthly evaporation pan coefficient	decimal fraction	0.2-2.0	1.09
fastcoef_lin	Linear coefficient in equation to route preferential flow storage down slope for each HRU	fraction/day	1E-5-0.1	0.07
fastcoef_sq	Non-linear coefficient in equation to route preferential flow storage down slope for each HRU	(-)	1E-5-0.1	0.05
gwflow_coef	Linear coefficient in the equation to compute groundwater discharge for each Groundwater reservoir (GWR)	fraction/day	1E-5-0.005	0.005
gwsink_coef	Linear coefficient in the equation to compute outflow to the groundwater sink for each GWR	fraction/day	0.0-0.2	0.15
hru_percent_imperv	Fraction of each HRU that is impervious	decimal fraction	0.0-0.1	2E-4
imperv_stor_max	Maximum impervious area retention storage for each HRU	inches	0.01-0.1	0.9
rain_adj	Monthly adjustment factor to adjust precipitation distributed to each HRU to account for difference in elevation, spatial variation, topography, and gage catch efficiency	decimal fraction	0.75-1.2	0.75
sat_threshold	Water holding capacity of the gravity and preferential flow reservoirs; difference between field capacity and total soil saturation for each HRU	inches	1.0-100.0	71.29
slowcoef_lin	Linear coefficient in equation to route gravity reservoir storage down slope for each HRU	fraction/day	0.001-0.5	0.05
slowcoef_sq	Non-linear coefficient to route gravity reservoir storage down slope for each HRU	(-)	0.001-0.5	0.12
smidx_coef	Coefficient in nonlinear contributing area algorithm for each HRU	(-)	0.001-0.06	1.0E-3
smidx_exp	Exponent in non-linear contributing area algorithm for each HRU	1/inch	0.1-0.5	0.19
soil_moist_max	Maximum available water holding capacity of capillary reservoir from land surface to rooting depth of the major vegetation type of each HRU.	inches	0.001-10.0	5.18
soil_rechr_max	Maximum storage for soil recharge zone (upper portion of capillary reservoir where losses occur as both evaporation and transpiration).	inches	0.001-5.0	0.015
soil2gw_max	Maximum amount of the capillary reservoir excess that is routed directly to the GWR for each HRU	inches	0.0-5.0	4.38
srain_intcp	Summer rain interception storage capacity for the major vegetation type on an HRU	inches	0.0-1.0	0.56
ssr2gw_exp	Non-linear coefficient in equation to route water from the gravity reservoirs to the GWR for each HRU	(-)	0.0-3.0	2.10
ssr2gw_rate	Linear coefficient in equation used to route water from the gravity reservoir to the GWR for each HRU	fraction/day	0.05-0.08	0.18
ssrcoef_lin	Coefficients to route subsurface storage to stream flow	fraction/day	0.0-1.0	0.32
ssrcoef_sq	Coefficients to route subsurface storage to stream flow	(-)	0.0-1.0	0.64
ssrmax_coef	Coefficient to route water from the subsurface reservoirs to the groundwater reservoirs	inches	1.0-20.0	2.50
wrain_intcp	Winter rain interception storage capacity for the major vegetation type on an HRU	inches	0.0-1.0	0.65

[a] In total, 32 parameters were adjusted during the calibration. Acceptable parameter ranges were directly obtained from PRMS IV support document (Markstrom et al., 2015) and modfied in some cases. Mean value for all HRUs were calibrated for all paramters.

S10. Sensitivity analysis

MODFLOW-OWHM parameter sensitivity analysis was carried out using PEST. Sensitivities are calculated as the derivatives of change in simulated head to change in parameter. Observations, like groundwater levels, are likely to be very useful in estimating parameter value if their simulated equivalents change significantly for a small change in parameter value (Hill and Tiedeman, 2006). According to Hill and Tiedeman (2006), since sensitivities are measured in units of the simulated value divided by the units of the parameters, both of which may vary considerably, it is important to compare the relative importance of different observations using a common scale. Composite scale sensitive parameter is one of the dimensionless sensitivity parameters that is used to determine the aggregate information provided by the observations for the estimation of one parameter (Hill and Tiedeman, 2006). Ten parameters were selected for the sensitivity analysis. During the sensitivity analysis, each parameter value was increased by 50%, one at a time, while keeping the other parameter values unchanged. The output from the sensitivity analysis was used to calculate the composite relative sensitivity (Fig. S10). Hydraulic conductivity and specific storage of the second layer were found to be very sensitive. Specific storage of the second layer is the most sensitive parameter of all.

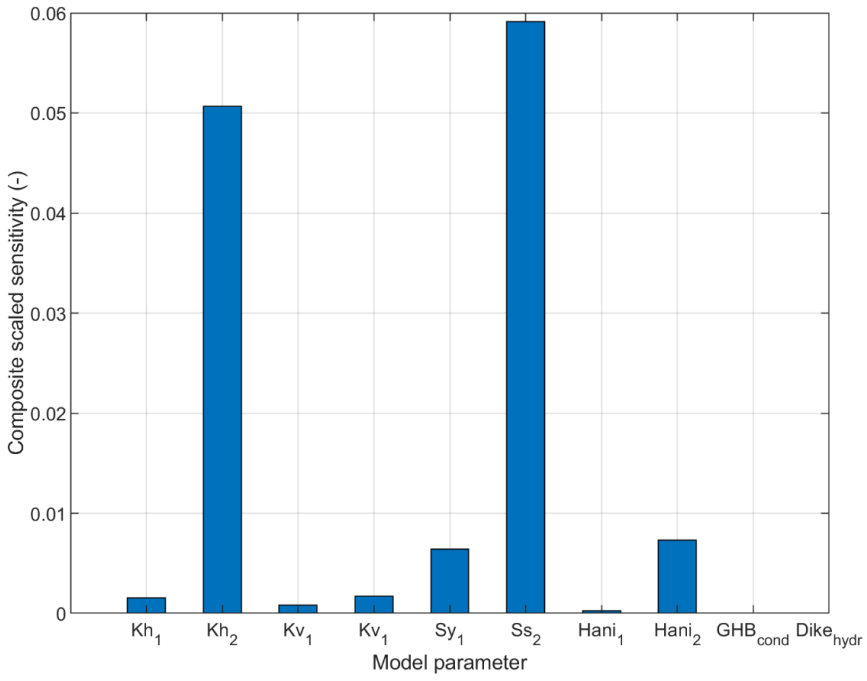

Fig. S10. Composite-scaled parameter sensitivities calculated by PEST using water level data from 10 observation wells in the Hout catchment.

S11. MODFLOW-OWHM model calibration and validation

The initial specified likely parameter range and final calibrated values are presented in Table S7. Specific storage for the second layer was calibrated using the pilot point (Fig. S11) while other parameters were calibrated assuming spatially uniform constant values. The 24 pilot points used for specific storage coefficient calibration and calibrated values are shown in Fig. S11. Table S8 presents the Mean Absolute Error (MAE) and Root Mean Square Error (RMSE) for four selected wells during the calibration and validation period. These wells were selected due to their continuous and long-term observation records.

Table S7. Parameters selected for calibration and their calibrated values.

Parameter	Units	Initial	Lower bound [a]	Upper bound [a]	Calibrated
Kh_1	m/d	0.38	$2.0x10^{-2}$	3.0	0.41
Kh_2	m/d	0.71	$2.0x10^{-2}$	3.0	0.86
Kv_1	m/d	$3.8x10^{-2}$	$1.0x10^{-3}$	3.0	1.23
Kv_2	m/d	$7.1x10^{-2}$	$2.0x10^{-3}$	3.0	0.83
Sy_1	(-)	0.1	0.01	0.25	0.01
Sy_2	(-)	0.1	0.01	0.25	0.05
Ss_2	1/m	$2.5x10^{-3}$	$1.0x10^{-3}$	$8.5x10^{-3}$	Calibrated with pilot point
$Hani_1$	(-)	0.1	$1.0x10^{-2}$	1.0	1.0
$Hani_2$	(-)	0.1	$1.0x10^{-2}$	1.0	0.1
GHB_{cond}	m^2/d	$3.0x10^{2}$	$1.0x10^{-3}$	$3.0x10^{4}$	$3.0x10^{3}$
$Dike_{hydr}$	1/d	$1.0\ x10^{-5}$	$1.0\ x10^{-20}$	$1.0\ x10^{-3}$	$1.0\ x10^{-20}$
Kvr_{124}	m/d	$1.0\ x10^{-2}$	$1.0\ x10^{-3}$	3.0	0.0145
Kvr_{35}	m/d	$2.0\ x10^{-2}$	$1.0\ x10^{-3}$	3.0	0.0177
n_{124}	(-)	0.12	0.01	0.3	0.10
n_{35}	(-)	0.2	0.01	0.3	0.15

[a] Lower and upper bound represent the realistic minimum and maximum parameter values used to constrain model calibration

Table S8. MAE and RMSE during the calibration and validation period.

Observation well ID	Calibration		Validation	
	MAE	RMSE	MAE	RMSE
A7N0524	0.42	0.50	0.51	3.35
A7N0641	4.00	4.04	3.24	3.35
A7N0644	2.18	2.25	3.23	3.30
A7N0635	1.07	1.14	0.91	0.94

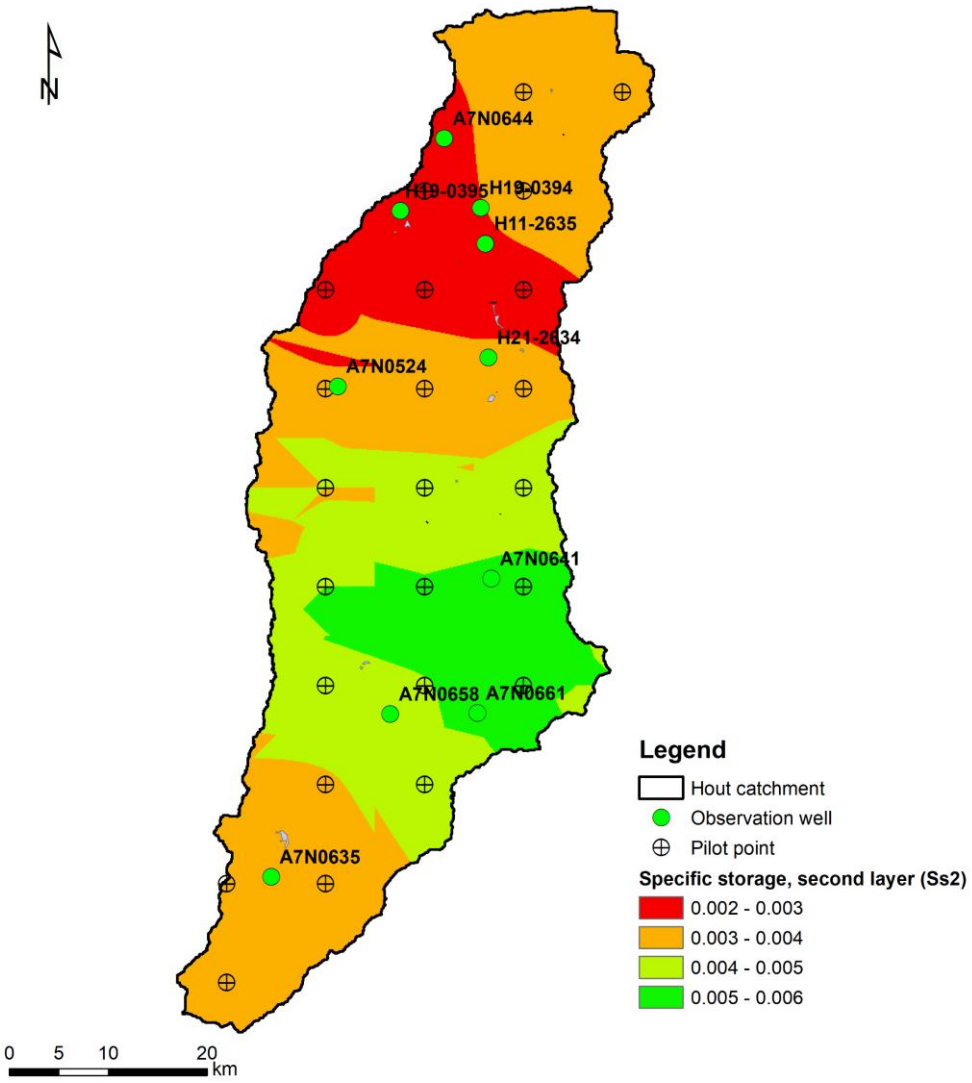

Fig. S11. Specific storage for layer 2 calibrated using pilot point calibration method.

S12. Evapotranspiration from groundwater

Evapotranspiration from groundwater (GW_{ET}) was calculated for Feb 2015 (validation period). The relevant parameter is Net recharge to groundwater (R_n). It will be negative when evapotranspiration occurs and gives the amount leaving the storage by this mechanism. The cell-by-cell figures were exported to a shape file, and total area with negative R_n was calculated. The area where GW_{ET} occurs during the selected stress period was found to be 4405 ha. GW_{ET} mainly occurs along the river downstream of the Hout River dam (Fig. S12).

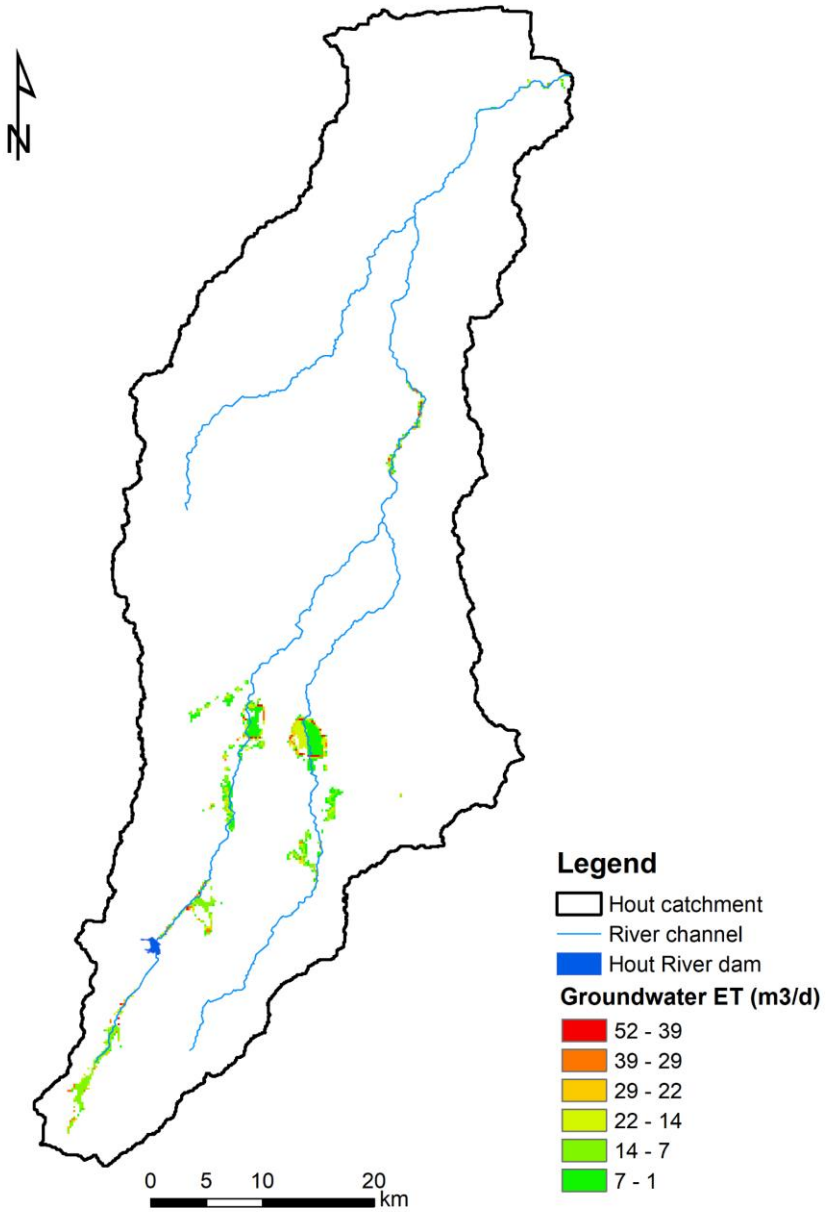

Fig. S12. Cell-by-cell evapotranspiration from groundwater (GW_{ET}) (m^3/d) during Feb 2015

ESM References

Ajami H, McCabe M, Evans J (2015) Impacts of model initialization on an integrated surface water–groundwater model. Hydrological Processes 29: 3790-3801

Anderson M, Woessner W (2002) Applied Groundwater Modeling: Simulation of Flow and Advective Transport. Acadenuc Press; 1 edition (Dec 11 1991) Academic Press, San Diego.

Arcement G, Schneider V (1989) Guide for selecting Manning's roughness coefficients for natural channels and flood plains US Government Printing Office Washington, DC.

Barlow P, Dickerman D (2001) Numerical-simulation and conjunctive-management models of the Hunt-Annaquatucket-Pettaquamscutt stream-aquifer system, Rhode Island US Geological Survey

Harbaugh A (2005) MODFLOW-2005, the US Geological Survey modular ground-water model: the ground-water flow process US Department of the Interior, US Geological Survey Reston, VA, USA

Hassan S, Lubczynski M, Niswonger R, Su Z (2014) Surface–groundwater interactions in hard rocks in Sardon Catchment of western Spain: An integrated modeling approach. Journal of Hydrology 517: 390-410

Hill M, Tiedeman C (2006) Effective groundwater model calibration: with analysis of data, sensitivities, predictions, and uncertainty. John Wiley & Sons

Jolly J (1986) Borehole/Irrigation survey and Ground-water Evaluation of the Doringlaagte Drainage Basin Dendron Directorate: Geohydrology, Department of Water Affairs, Gh Report No. 3495.

Jones A, Breuning-Madsen H, Brossard M, Dampha A, Deckers J, Dewitte O, Gallali T, Hallett S, Jones R, Kilasara M (2013) Soil Atlas of Africa, European Commission

Kallel A, Ksibi M, Dhia H, Khélifi N (2017) Recent Advances in Environmental Science from the Euro-mediterranean and Surrounding Regions: Proceedings of Euro-mediterranean Conference for Environmental Integration (emcei-1), Tunisia 2017 Springer

Leavesley G, Lichty R, Thoutman B, Saindon L (1983) Precipitation-runoff modeling system: User's manual USGS Washington, DC

Lemieux J, Sudicky E, Peltier W, Tarasov L (2008) Dynamics of groundwater recharge and seepage over the Canadian landscape during the Wisconsinian glaciation. Journal of Geophysical Research: Earth Surface 113

Liu H, Hsu N, Lee T (2009) Simultaneous identification of parameter, initial condition, and boundary condition in groundwater modelling. Hydrological processes 23: 2358-2367

Lloyd J (1981) Case-studies in groundwater resources evaluation, Clarendon Press

Markstrom S, Regan R, Hay L, Viger R, Webb R, Payn R, LaFontaine J (2015) PRMS-IV, the precipitation-runoff modeling system, version 4, US Geological Survey.

Nash J, Sutcliffe J (1970) River flow forecasting through conceptual models part I—A discussion of principles. Journal of hydrology 10: 282-290

Niswonger R, Prudic D (2005) Documentation of the Streamflow-Routing (SFR2) Package to include unsaturated flow beneath streams-A modification to SFR1, US Geological Survey.

Pervez M, Budde M, Rowland J (2014) Mapping irrigated areas in Afghanistan over the past decade using MODIS NDVI. Remote Sensing of Environment 149: 155-165

Prudic D, Konikow L, Banta E (2004) A new streamflow-routing (SFR1) package to simulate stream-aquifer interaction with MODFLOW-2000, Open-File Report 2004-1042, USGS

Schmid W, Hanson R, Maddock III T, Leake S (2006) User guide for the farm process (FMP1) for the US Geological Survey's modular three-dimensional finite-difference ground-water flow model, MODFLOW-2000. US Geological Survey Techniques and Methods: 6-A17